Inorganic Chemistry

pubs.acs.org/IC

Article

Thinking about the Box: Exploring the Electronic Structure of a Cuboidal-Shaped Mo_{84} Anionic Nanocapsule

Published as part of Inorganic Chemistry special issue "Forum on Polyoxometalate and Metal-Oxo Chemistry".

Diego Garay-Ruiz, Jordi Buils, Nuno A. G. Bandeira, Sebastien Floquet, Emmanuel Cadot, and Carles Bo*

Cite This: *Inorg. Chem.* 2025, 64, 2716–2722

Read Online

ACCESS | Metrics & More | Article Recommendations | Supporting Information

ABSTRACT: The cubic-shaped polyoxothiomolybdate $[Mo_{84}O_{188}S_{48}(AcO)_{24}]^{40-}$ first reported by Cadot and collaborators has been characterized by DFT methods for the first time, elucidating its electronic structure by means of the analysis of the density of states as well as its frontier molecular orbitals. Moreover, the electron density of this complex molecular oxo-cluster has been studied through QTAIM analysis, focusing on the characteristic Mo(V)−Mo(V) bonding pattern appearing at the corner subunits of the nanocapsule.

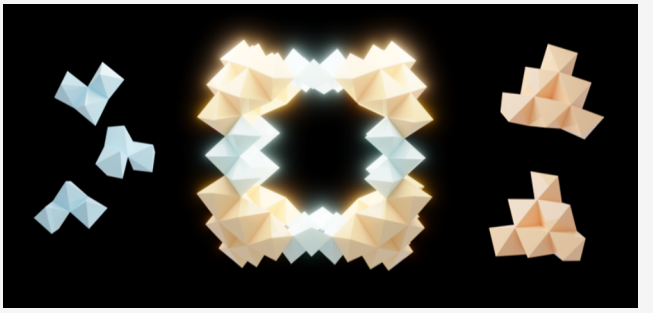

INTRODUCTION

The chemistry of polyoxometalates (POMs) is characterized by their deep structural richness, with a relatively low number of building block motifs being able to assemble in a wide variety of complex, highly symmetric structures.[1] One of the most striking examples of this behavior is the molybdenum $\{Mo_{132}\}$ Keplerate anion first identified by Achim Müller and co-workers[2] in 1998. The spherical nanocluster (Figure 1) is formed by the combination of 12 Mo(VI)-based pentagonal $\{Mo_6O_{21}\}$ subunits and 30 Mo(V) dimeric $\{Mo_2O_2(\mu\text{-}O_2)\}$ linkers arranged as the vertices and edges of a dodecahedron, respectively. From there, modifying the composition of these blocks enabled the synthesis of a whole family of compounds like the heterometallic $\{Mo_{72}Fe_{30}\}$,[3] the $\{Mo_{102}\}$ oxo-cluster,[4] and other related species.[4−9] This kind of highly symmetrical arrangement of few components can be also found in the capsids of viruses and in computationally designed megadalton protein complexes.[9,10]

Apart from their remarkable structures, this class of molecular nanocages showcase relevant properties such as the ability to encapsulate organic molecules[11,12] and to tune the properties of confined water,[13] with applications in catalysis,[14−19] medicine,[20] and energy.[21,22] Numerous recent studies are being focused on exploiting the promising properties of this kind of nanocapsules toward the design of novel materials.[23]

In this context, the sulfur analogue of the $\{Mo_{132}\}$ nanocapsule was synthesized back in 2011 by an international team lead by Achim Müller, replacing the oxygen-based linkers by $[Mo^{V}_{2}O_2(\mu\text{-}S)_2]$ subunits.[24] Furthermore, a study by the Versailles (France) team[25] demonstrated that in a narrow range of pH, either this sulfurated Keplerate anion or a novel cubic-shaped $\{Mo_{84}\}$ molecular cluster with D_{2h} point group symmetry can be produced. This cuboidal structure (see Figure 1) was formed by 8 hexameric Mo(V) units in the corners of the cube, built each from 3 $[Mo^{V}_{2}O_2(\mu\text{-}S)_2]$ building blocks, brought together by 12 trimeric Mo(VI) subunits in every edge.

The final polyoxothiomolybdate $[Mo_{84}O_{188}S_{48}(AcO)_{24}]^{40-}$ was isolated as an octahedral yellow crystal including both Na^+ and NMe_4^+ counterions, as well as additional noncoordinated acetate and a very large number of hydration water molecules. Nonetheless, most of these components are strongly disordered in the crystal lattice, where only the main $\{Mo_{84}\}$ unit and a few water molecules and counter cations could be uniquely identified. On the one hand, it is still unclear whether the capsule stability is dictated by the cations and water molecules inside or by the structure itself. On the other hand, the bonding within the new triangular hexameric Mo(V) units, which derives from the dimer holding a Mo(V)−Mo(V) metal−metal bond, has not been described yet.

Received: October 22, 2024
Revised: January 15, 2025
Accepted: January 23, 2025
Published: January 30, 2025

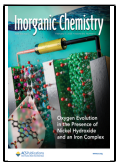

https://doi.org/10.1021/acs.inorgchem.4c04497
Inorg. Chem. 2025, 64, 2716−2722

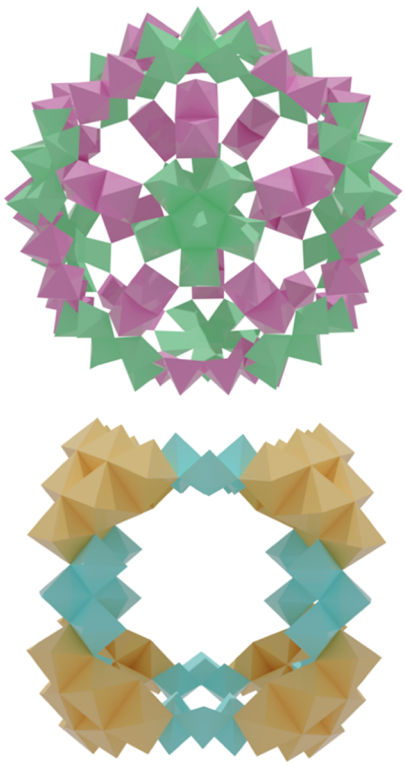

Figure 1. Polyhedral representations of the spheroidal $\{Mo_{132}\}$ Keplerate anion (above) and the cuboidal $\{Mo_{84}\}$ analogue (below). Building blocks are color-coded: green for pentagonal $\{Mo_6^{VI}\}$, pink for dimeric $\{Mo_2^{V}\}$, orange for $\{Mo_6^{V}\}$ corners, and blue for $\{Mo_3^{VI}\}$ edges.

While the role of computational chemistry in elucidating the behavior, reactivity, and even the self-assembly processes of POMs has been paramount,[26−32] the high charge and very large size of Keplerate-like anions have limited in silico studies focusing on them. Nonetheless, existing studies have provided relevant insights on the electronic structure[33−35] or the water-organizing properties[36−38] of this kind of nanoclusters.

Thereby, in this study, we aimed to characterize the electronic structure of the $\{Mo_{84}\}$ cuboidal polyoxothiomolybdate by means of a DFT-based method. Apart from the nature of the molecular orbitals, we also explored the bonding patterns in the cluster, with a special focus on the Mo(V)−Mo(V) bonds expected for these d^1 cationic atoms. To contextualize this analysis, we compared the electronic structure and bonding of this structure with those of the spherical $\{Mo_{132}\}$ Keplerate nanocapsule, evaluating the similarities and differences between these two giant POM arrangements.

RESULTS

As a starting point, we optimized the fully deprotonated $[Mo_{84}O_{188}S_{48}(AcO)_{24}]^{40-}$ empty molecular structure, including 12 hydration water molecules interacting with the Mo(VI) trimers in the edge of the cube. For the sake of comparison, we also optimized the spheroidal $[Mo_{132}O_{312}S_{60}]^{12-}$ Keplerate anion, in this case without water molecules. From here, we determined the total density of states (DOS) of the system between −25 and 10 eV, together with the corresponding gross population DOS for the Mo, S, and O atoms in the POM scaffold, as well as for the water and acetate groups. In the case of Mo, we also differentiated between Mo(VI) (cube edges for $\{Mo_{84}\}$ and pentagonal subunits for $\{Mo_{132}\}$) and Mo(V) (cube corners for $\{Mo_{84}\}$ and linkers for $\{Mo_{132}\}$). The complexity of the overall electronic structure of the metal-thio-oxo clusters is clear; however, the decomposition represented in Figure 2 brings to light several interesting features. In the case of the cuboidal nanocluster, two distinct peaks can be directly assigned to the acetate ligands absent in the spherical analogue. The s-bands of the sulfur atoms appear around the same region for both structures, although they are more stabilized in the case of $\{Mo_{132}\}$. The region between approximately −10 and −5 eV is quite complex and combines contributions of most atoms, although in general, it is dominated by the p-band of the scaffold oxygens and is also a bit lower for the spherical Keplerate. Although the peaks are not too clear when looking at the full DOS, the HOMO of the

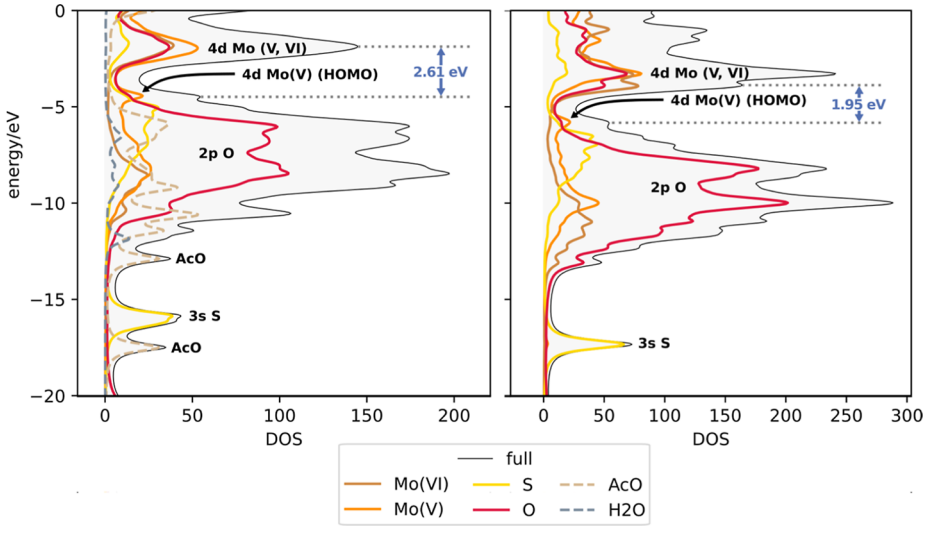

Figure 2. Total DOS and partial gross population DOS for cuboidal (left) and spheroidal (right) Keplerate anions. Red line corresponds to the contribution of the O atoms in the polyoxothiomolybdate scaffold, not including atoms belonging to additional species (water or acetate anions). Mo contribution has been split between Mo(VI) (edges, dark brown) and Mo(V) (corners, orange).

https://doi.org/10.1021/acs.inorgchem.4c04497
Inorg. Chem. 2025, 64, 2716−2722

system mostly corresponds to the 4d orbitals of the Mo(V) atoms for both structures, comprising the corners of the cube and the linkers of the sphere. Both entities show defined band gaps going from the HOMO region to a LUMO-associated peak, with the value for $\{Mo_{84}\}$ (ΔE = 2.6 eV) being remarkably larger than for $\{Mo_{132}\}$ (ΔE = 2.0 eV). This LUMO region, in both cases, combines the 4d bands of both types of molybdenum atoms as well as some p orbitals from oxygen. Nevertheless, the peak for the spherical Keplerate is more defined, showing two local maxima with the first being mainly associated with Mo(VI). From there, the assignment becomes much more diffuse as higher-energy virtual orbitals are reached.

To enhance the analysis of the less studied cuboidal Keplerate and despite the band-like structure associated with the very large number of molecular orbitals, we inspected the shape of the frontier orbitals (Figure 3), as well as the

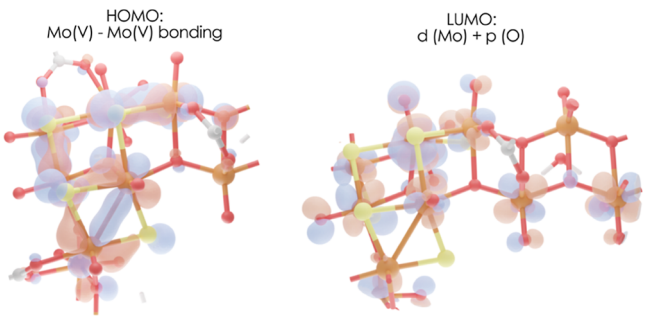

Figure 3. Depiction of the frontier molecular orbitals in the cuboidal Keplerate with isosurface value = 0.01, focusing on key regions of the highly symmetric structure. The HOMO (left) only pertains to the Mo(V)-based corners, while the LUMO (right) extends through Mo(V) corners and Mo(VI) edges.

corresponding HOMO−LUMO gap from discrete levels (1.7 eV, remarkably lower than the peak-to-peak band gap). This value is also in line with the orbital-to-orbital HOMO−LUMO gap for the icosahedral Keplerate[35] (1.5 eV). Figure 3 confirms the assignment of the HOMO to Mo(V) atoms in the hexameric corners, mostly showing bonding character across the Mo−Mo bonds. In contrast, the LUMO is formed by the d-orbitals of both types of Mo atoms in the scaffold as well as p orbitals from oxygen atoms (bridging and oxo). In any case, due to the numerous near-degenerate levels throughout the whole electronic structure, the DOS analysis and its decomposition (Figure 2) still provide a richer picture of the system.

As the structure characterized by Cadot and co-workers[25] was indeed an octaprotonated scaffold with a net −32 charge, we added the corresponding capping hydrogen atoms. The placement of these protons was made maintaining the D_{2h} symmetry point group to ensure the consistency of the molecular orbital symmetry, thus adding one H atom for each of the eight corner subunits. Then, we computed both the total DOS of this system and the contribution of the added protons, as depicted in Figure 4. The band structure of the 8H structure is very similar to that of the 0H anion, only that being shifted to slightly lower energies. A noteworthy feature is how the well-defined shoulder associated with the HOMO of the 0H structure (Mo(V) in corners) is more diffuse in the 8H DOS. Regarding the states associated with the actual protons, they

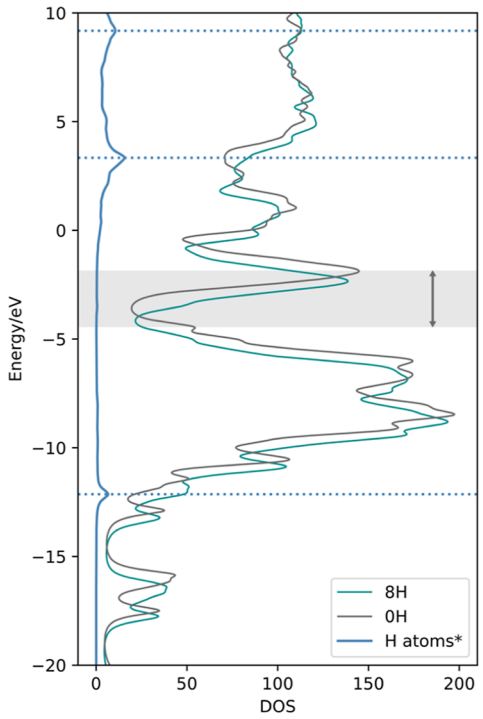

Figure 4. Total DOS for unprotonated (gray) and protonated (green) cuboidal anions. The contribution of the 8 protons (blue trace) has been scaled for visibility, with location of maxima highlighted with dotted lines. The HOMO−LUMO gap of the unprotonated structure is shaded in gray for reference.

appear quite far from the HOMO−LUMO region, with the two major peaks being below −10 eV and close to 5 eV.

Another relevant aspect to be discussed is the actual connectivity of the POM structure: Mo(V) entities, like in the "classical" spheroidal Mo_{132} Keplerate anion, are known to show Mo(V)−Mo(V) bonding through the remaining electron in their 4d-shell.

To explore this behavior, we carried out a QTAIM (quantum theory of atoms in molecules) analysis[39,40] of the topology of the electron density over the previous structure, thus unambiguously characterizing all covalent bonds in the cluster. Our calculations confirm the expected bonding patterns with BCPs being identified for the hexameric $\{Mo_6O_7S_6\}$ subunits in the corners (Figure 5). Thus, each corner has three Mo(V)−Mo(V) bonds, with every Mo atom in the fragment being paired with another. In contrast, the trimeric $\{Mo_3O_{11}\}$ subunits from the edges do not showcase any metal−metal bonding.

Furthermore, we analyzed the topological parameters at the BCPs (Table 1), comparing the cuboidal Keplerate to both the spherical analogue and to a model $[Mo_2O_2S_2(H_2O)_6]^{2+}$ dimer providing a minimal example of Mo(V)−Mo(V) bond. From the available QTAIM descriptors, we selected the electron density ($\rho(r)$), its Laplacian ($\nabla^2(\rho)$), the ellipticity (ε) of the bond, indicating the deviation of the electron density from a plane containing the bond path, and the total energy density (H_b). Additional parameters for the three systems, such as the decomposition of the energy in kinetic (G_b) and potential (V_b) energies, are available in the Supporting Information. While in general the Mo(V)−Mo(V) bond, across all three systems, is shown to be weaker than the metal−heteroatom bonds, it is present and preserved across the two explored arrangements

https://doi.org/10.1021/acs.inorgchem.4c04497
Inorg. Chem. 2025, 64, 2716−2722

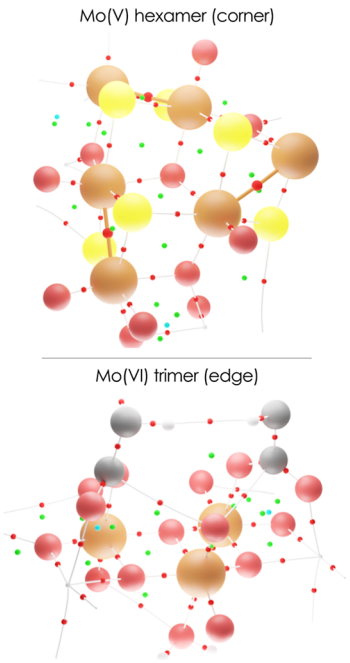

Figure 5. Tridimensional representation of QTAIM critical points and bond paths. Left, corner unit (Mo_6^V) and right, edge unit (Mo_3^{VI}). Color coding for atoms (larger spheres): Mo (orange), S (yellow), oxygen (red), carbon (gray), and hydrogen (white). Color coding for CPs (smaller spheres): bond (red), ring (green), and cage (cyan). Characteristic Mo(V)−Mo(V) interactions have been highlighted with thicker orange lines and larger BCPs.

(spheroidal and cuboidal). Moreover, it is also clearly stronger (larger electron density, Laplacian, and total energy) than an O−H hydrogen bond (Table S2 in Supporting Information), and very similar in terms of ρ and H_b to the Mo^V−O bond. An interesting feature is the very large ellipticity of this type of bond: while this deviation from the bond plane is very close to zero for all Mo−O and Mo−S bonds, it is already remarkable for the dimer (1.23) and increases significantly for the {Mo_{84}} (2.44) and the {Mo_{132}} (3.59) nanoclusters. Thus, the distribution of electron density across Mo(V)−Mo(V) bonds is shown to be fundamentally different than for "traditional" bond types.

Furthermore, we compared the geometries of the DFT-optimized structure and the X-ray structure characterized by Cadot and co-workers. Considering the very symmetric character of the Mo_{84} cluster, we selected key geometric parameters of the underlying cube: the height (distance between opposite faces), the diagonal of the cube, and the diagonal of the face, as well as the Mo(V)−Mo(V) distances for bonded molybdenum atoms in the corners.

A schematic representation of these distances is depicted in Figure 6, while the actual numeric values are collected in Table 2.

There is a certain degree of expansion of the cubic structure from the crystal structure to the relaxed DFT geometry, with the diagonal d_{CC} increasing by 1.0 Å. Nonetheless, the overall changes are quite small, showcasing the consistency between experimental and computational results. Regarding Mo(V)−Mo(V) bonding, we also observe a quite small enlargement (0.05 Å), consistent with the general trend.

Table 1. Selected QTAIM Parameters (Electron Density, Bond Ellipticity, Laplacian, and Total Energy Density, All in Atomic Units) at BCPs of Representative Bond Types in {Mo_2}, {Mo_{132}}, and {Mo_{84}} Oxo-Clusters[a]

	bond	{Mo_2}	{Mo_{132}}	{Mo_{84}}
ρ	Mo^V−Mo^V	0.06 ± 0.00	0.05 ± 0.00	0.05 ± 0.00
	Mo^V−O	0.06 ± 0.01	0.09 ± 0.00	0.08 ± 0.01
	Mo^{VI}−O		0.16 ± 0.03	0.13 ± 0.01
	Mo^V=O	0.25 ± 0.00	0.25 ± 0.00	0.23 ± 0.00
	Mo^{VI}=O		0.24 ± 0.00	0.22 ± 0.01
	Mo^V−S	0.10 ± 0.00	0.10 ± 0.00	0.08 ± 0.02
ε	Mo^V−Mo^V	1.23 ± 0.00	3.59 ± 0.00	2.44 ± 0.01
	Mo^V−O	0.17 ± 0.09	0.14 ± 0.00	0.10 ± 0.07
	Mo^{VI}−O		0.08 ± 0.03	0.07 ± 0.02
	Mo^V=O	0.00 ± 0.00	0.00 ± 0.00	0.01 ± 0.01
	Mo^{VI}=O		0.00 ± 0.00	0.02 ± 0.01
	Mo^V−S	0.15 ± 0.02	0.13 ± 0.00	0.22 ± 0.07
$\nabla^2(\rho)$	Mo^V−Mo^V	0.04 ± 0.00	0.04 ± 0.00	0.03 ± 0.00
	Mo^V−O	0.25 ± 0.05	0.41 ± 0.00	0.31 ± 0.05
	Mo^{VI}−O		0.62 ± 0.17	0.48 ± 0.04
	Mo^V=O	0.90 ± 0.00	0.85 ± 0.00	0.87 ± 0.01
	Mo^{VI}=O		0.84 ± 0.01	0.81 ± 0.02
	Mo^V−S	0.14 ± 0.00	0.13 ± 0.00	0.12 ± 0.02
H_b	Mo^V−Mo^V	−0.02 ± 0.00	−0.02 ± 0.00	−0.02 ± 0.00
	Mo^V−O	−0.01 ± 0.00	−0.02 ± 0.00	−0.02 ± 0.01
	Mo^{VI}−O		−0.08 ± 0.02	−0.06 ± 0.01
	Mo^V=O	−0.20 ± 0.00	−0.21 ± 0.00	−0.17 ± 0.00
	Mo^{VI}=O		−0.20 ± 0.01	−0.16 ± 0.01
	Mo^V−S	−0.05 ± 0.00	−0.05 ± 0.00	−0.04 ± 0.01

[a]Values correspond to the average property among all bonds of the same type ± the standard deviation (note that some values of the standard deviation are very small).

https://doi.org/10.1021/acs.inorgchem.4c04497
Inorg. Chem. 2025, 64, 2716−2722

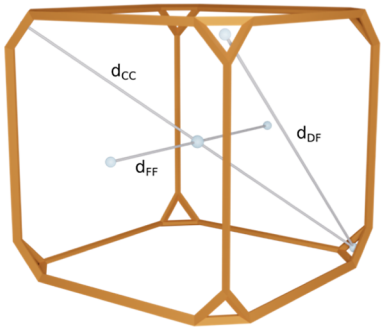

Figure 6. Simplified representation (truncated cube) of the studied molecule. Selected distances are represented by lines (d_{CC}: distance from corner to opposite corner; d_{FF}: distance from face to opposite face; and d_{DF}: distance of the diagonal of the face).

Table 2. Selected Average Distances and Standard Deviations, in Angstroms (Note That Some Standard Deviation Values are Very Small)

	length (Å) (X-ray)	length (Å) (DFT)
d_{FF}	14.47 ± 0.41	14.70 ± 0.12
d_{CC}	21.10 ± 0.00	22.13 ± 0.00
d_{DF}	17.22 ± 0.00	18.07 ± 0.00
$d(Mo^{V}–Mo^{V})$	2.83 ± 0.00	2.88 ± 0.00

CONCLUSIONS

POM chemistry is associated with a wide variety of structural motifs, of huge interest from both experimental and computational points of view. In this work, we have characterized the $\{Mo_{84}\}$ cuboidal cluster in silico for the first time, providing valuable insights about its electronic structure, such as the comparability of its band gap with the analogous $\{Mo_{132}\}$ spheroidal Keplerate anion, and the distinct participation of Mo^{V} and Mo^{VI} atoms to the main bands in the spectrum. Additionally, we have also identified the bonding character of the Mo(V)−Mo(V) entities appearing in the corners of the cube, comparing the bonding parameters extracted from QTAIM with those of a model dimeric structure and the spheroidal analogue, contextualizing the strength and particularities of this metal−metal bond. Finally, we have also compared key structural parameters between the crystal structure, isolated experimentally, and the DFT-optimized structure, confirming the low degree of deviation between them. All in all, we provide unprecedented insights about the stability and bonding pattern of this molybdenum oxysulfide nanocapsule, paving the way for further studies on this scarcely explored type of the system. We very much hope that this work serves as a testament to Achim Müller's enthusiasm and sense of wonder for the beauty and symmetry of these complex systems which he so easily imparted to his colleagues and friends.

COMPUTATIONAL DETAILS

For the DFT characterization of the cubic Keplerate unit, we employed the AMS 2021 software,[41] with the BP86[42−44]/TZP level of theory and ZORA[45,46] relativistic corrections. The numerical quality was set to "good", the frozen core to "small", and the COSMO[47] solvation model was employed, using the default parameters for water and Klamt radii. DOS calculations were also carried out in AMS 2021, with a Lorentzian width of 0.25 eV. A collection of the produced computational results is available in the ioChem-BD repository[48] and can be accessed through the following link 10.19061/iochem-bd-1-353.

ASSOCIATED CONTENT

Supporting Information

The Supporting Information is available free of charge at https://pubs.acs.org/doi/10.1021/acs.inorgchem.4c04497.

QTAIM properties of selected systems (PDF)

AUTHOR INFORMATION

Corresponding Author

Carles Bo − *Institute of Chemical Research of Catalonia (ICIQ), Tarragona 43007, Spain; Departament de Química Física i Inorgànica, Universitat Rovira i Virgili, Tarragona 43007, Spain;* orcid.org/0000-0001-9581-2922; Email: cbo@iciq.cat

Authors

Diego Garay-Ruiz − *Institute of Chemical Research of Catalonia (ICIQ), Tarragona 43007, Spain;* orcid.org/0000-0003-0744-0562

Jordi Buils − *Institute of Chemical Research of Catalonia (ICIQ), Tarragona 43007, Spain; Departament de Química Física i Inorgànica, Universitat Rovira i Virgili, Tarragona 43007, Spain*

Nuno A. G. Bandeira − *Biosystems and Integrative Sciences Institute (BioISI)—Departamento de Química e Bioquímica, Faculdade de Ciências, Universidade de Lisboa, Lisboa 1749-016, Portugal;* orcid.org/0000-0002-5754-7328

Sebastien Floquet − *Institut Lavoisier de Versailles, UMR 8180 CNRS, UVSQ, Université Paris-Saclay, Versailles 78035, France;* orcid.org/0000-0003-2433-1771

Emmanuel Cadot − *Institut Lavoisier de Versailles, UMR 8180 CNRS, UVSQ, Université Paris-Saclay, Versailles 78035, France;* orcid.org/0000-0003-4136-6298

Complete contact information is available at: https://pubs.acs.org/10.1021/acs.inorgchem.4c04497

Author Contributions

All authors have given approval to the final version of the manuscript.

Notes

The authors declare no competing financial interest.

ACKNOWLEDGMENTS

We acknowledge the Spanish Ministry of Science, Innovation and Universities MCIN/AEI/10.13039/501100011033 for the projects PID2023-153344NB-I00, PID2020-112806RB-I00, and CEX2019-000925-S. We also thank the European Union NextGenerationEU/PRTR (TED2021-132850B−I00), the ICIQ Foundation, and the CERCA program of the Generalitat de Catalunya. BioISI acknowledges Fundação para a Ciência e a Tecnologia (FCT) for financial support (UID/04046/2025). N.A.G.B. acknowledges the FCT/DL57 researcher program for funding (doi: 10.54499/DL57/2016/CP1479/CT0050) and FCT grant PTDC/QUI-QIN/0252/2021 doi: 10.54499/PTDC/QUI-QIN/0252/2021.

REFERENCES

(1) Lunk, H.-J.; Hartl, H. The Fascinating Polyoxometalates. *ChemTexts* **2021**, 7 (4), 26.

(2) Müller, A.; Krickemeyer, E.; Bögge, H.; Schmidtmann, M.; Peters, F. Organizational Forms of Matter: An Inorganic Super Fullerene and Keplerate Based on Molybdenum Oxide. *Angew. Chem., Int. Ed.* **1998**, *37* (24), 3359−3363.
(3) Müller, A.; Sarkar, S.; Shah, S. Q. N.; Bögge, H.; Schmidtmann, M.; Sarkar, S.; Kögerler, P.; Hauptfleisch, B.; Trautwein, A. X.; Schünemann, V. Archimedean Synthesis and Magic Numbers: "Sizing" Giant Molybdenum-Oxide-Based Molecular Spheres of the Keplerate Type. *Angew. Chem., Int. Ed.* **1999**, *38* (21), 3238−3241.
(4) Müller, A.; Shah, S. Q. N.; Bögge, H.; Schmidtmann, M.; Kögerler, P.; Hauptfleisch, B.; Leiding, S.; Wittler, K. Thirty Electrons "Trapped" in a Spherical Matrix: A Molybdenum Oxide-Based Nanostructured Keplerate Reduced by 36 Electrons. *Angew. Chem., Int. Ed.* **2000**, *39* (9), 1614−1616.
(5) Müller, A.; Serain, C. Soluble Molybdenum Blues"Des Pudels Kern. *Acc. Chem. Res.* **2000**, *33* (1), 2−10.
(6) Müller, A.; Beckmann, E.; Bögge, H.; Schmidtmann, M.; Dress, A. Inorganic Chemistry Goes Protein Size: A Mo368 Nano-Hedgehog Initiating Nanochemistry by Symmetry Breaking. *Angew. Chem., Int. Ed.* **2002**, *41* (7), 1162−1167.
(7) Kögerler, P.; Tsukerblat, B.; Müller, A. Structure-Related Frustrated Magnetism of Nanosized Polyoxometalates: Aesthetics and Properties in Harmony. *Dalton Trans.* **2010**, *39* (1), 21−36.
(8) Todea, A. M.; Merca, A.; Bögge, H.; van Slageren, J.; Dressel, M.; Engelhardt, L.; Luban, M.; Glaser, T.; Henry, M.; Müller, A. Extending the $\{(Mo)Mo_5\}_{12}M_{30}$ Capsule Keplerate Sequence: A $\{Cr_{30}\}$ Cluster of $S = 3/2$ Metal Centers with a $\{Na(H_2O)_{12}\}$ Encapsulate. *Angew. Chem., Int. Ed.* **2007**, *46* (32), 6106−6110.
(9) Müller, A.; Todea, A. M.; Van Slageren, J.; Dressel, M.; Bögge, H.; Schmidtmann, M.; Luban, M.; Engelhardt, L.; Rusu, M. Triangular Geometrical and Magnetic Motifs Uniquely Linked on a Spherical Capsule Surface. *Angew. Chem., Int. Ed.* **2005**, *44* (25), 3857−3861.
(10) Bale, J. B.; Gonen, S.; Liu, Y.; Sheffler, W.; Ellis, D.; Thomas, C.; Cascio, D.; Yeates, T. O.; Gonen, T.; King, N. P.; Baker, D. Accurate Design of Megadalton-Scale Two-Component Icosahedral Protein Complexes. *Science* **2016**, *353* (6297), 389−394.
(11) Müller, A.; Krickemeyer, E.; Bögge, H.; Schmidtmann, M.; Botar, B.; Talismanova, M. O. Drawing Small Cations into Highly Charged Porous Nanocontainers Reveals "Water" Assembly and Related Interaction Problems. *Angew. Chem., Int. Ed.* **2003**, *42* (18), 2085−2090.
(12) Kopilevich, S.; Gottlieb, H.; Keinan-Adamsky, K.; Müller, A.; Weinstock, I. A. The Uptake and Assembly of Alkanes within a Porous Nanocapsule in Water: New Information about Hydrophobic Confinement. *Angew. Chem.* **2016**, *128* (14), 4552−4557.
(13) Mishra, P. P.; Pigga, J.; Liu, T. Membranes Based on "Keplerate"-Type Polyoxometalates: Slow, Passive Cation Transportation and Creation of Water Microenvironment. *J. Am. Chem. Soc.* **2008**, *130* (5), 1548−1549.
(14) Taghiyar, H.; Yadollahi, B. New Perspective to Catalytic Epoxidation of Olefins by Keplerate Containing Keggin Polyoxometalates. *Polyhedron* **2018**, *156*, 98−104.
(15) Taghiyar, H.; Yadollahi, B. Keggin Polyoxometalates Encapsulated in Molybdenum-Iron-Type Keplerate Nanoball as Efficient and Cost-Effective Catalysts in the Oxidative Desulfurization of Sulfides. *Sci. Total Environ.* **2020**, *708*, 134860.
(16) Liu, J.; Jiang, N.; Lin, J.; Mei, Z.; Dong, L.; Kuang, Y.; Liu, J.; Yao, S.; Li, S.; Lan, Y. Structural Evolution of Giant Polyoxometalate: From "Keplerate" to "Lantern" Type Mo_{132} for Improved Oxidation Catalysis. *Angew. Chem., Int. Ed.* **2023**, *62* (33), No. e202304728.
(17) Wang, P.; Wang, T.; Xu, M.; Gao, Z.; Li, H.; Li, B.; Wang, Y.; Qu, C.; Feng, M. Keplerate Polyoxomolybdate Nanoball Mediated Controllable Preparation of Metal-Doped Molybdenum Disulfide for Electrocatalytic Hydrogen Evolution in Acidic and Alkaline Media. *Chin. Chem. Lett.* **2024**, *35* (7), 108930.
(18) Krishnamoorthy, K.; Pazhamalai, P.; Swaminathan, R.; Mohan, V.; Kim, S. Unravelling the Bi-Functional Electrocatalytic Properties of $\{Mo_{72}Fe_{30}\}$ Polyoxometalate Nanostructures for Overall Water Splitting Using Scanning Electrochemical Microscope and Electrochemical Gating Methods. *Adv. Sci.* **2024**, *11*, 2401073.
(19) Haviv, E.; Chen, B.; Carmieli, R.; Houben, L.; Cohen, H.; Leitus, G.; Avram, L.; Neumann, R. Guest Transition Metals in Host Inorganic Nanocapsules: Single Sites, Discrete Electron Transfer, and Atomic Scale Structure. *J. Am. Chem. Soc.* **2020**, *142* (34), 14504−14512.
(20) Taghiyar, H.; Yadollahi, B.; Kajani, A. A. Controlled Drug Delivery and Cell Adhesion for Bone Tissue Regeneration by Keplerate Polyoxometalate (Mo132)/Metronidazole/PMMA Scaffolds. *Sci. Rep.* **2022**, *12* (1), 14443.
(21) Huang, S.-C.; Lin, C.-C.; Hsu, C.-T.; Guo, C.-H.; Chen, T.-Y.; Liao, Y.-F.; Chen, H.-Y. Keplerate-Type Polyoxometalate {Mo72Fe30} Nanoparticle Anodes for High-Energy Lithium-Ion Batteries. *J. Mater. Chem. A* **2020**, *8* (41), 21623−21633.
(22) Zhang, J.; Ma, C.; Hao, Y.; Chen, W. A Flexible Triboelectric Nanogenerator Based on TiO_2 Nanoarrays and Polyoxometalate for Harvesting Biomechanical Energy. *ACS Appl. Nano Mater.* **2024**, *7* (14), 16922−16931.
(23) Wang, K.; Iwano, T.; Uchida, S. Keplerate Polyoxometalate Compounds: A Multifunctional Nano-Platform for Advanced Materials. *Dalton Trans.* **2024**, *53*, 16797.
(24) Schäffer, C.; Todea, A. M.; Bögge, H.; Cadot, E.; Gouzerh, P.; Kopilevich, S.; Weinstock, I. A.; Müller, A. Softening of Pore and Interior Properties of a Metal-Oxide-Based Capsule: Substituting 60 Oxide by 60 Sulfide Ligands. *Angew. Chem., Int. Ed.* **2011**, *50* (51), 12326−12329.
(25) Bannani, F.; Floquet, S.; Leclerc-Laronze, N.; Haouas, M.; Taulelle, F.; Marrot, J.; Kögerler, P.; Cadot, E. Cubic Box versus Spheroidal Capsule Built from Defect and Intact Pentagonal Units. *J. Am. Chem. Soc.* **2012**, *134* (47), 19342−19345.
(26) Gil, A.; Carbó, J. J. Computational Modelling of the Interactions between Polyoxometalates and Biological Systems. *Front. Chem.* **2022**, *10*, 876630.
(27) Chen, J.-J.; Vilà-Nadal, L.; Solé-Daura, A.; Chisholm, G.; Minato, T.; Busche, C.; Zhao, T.; Kandasamy, B.; Ganin, A. Y.; Smith, R. M.; Colliard, I.; Carbó, J. J.; Poblet, J. M.; Nyman, M.; Cronin, L. Effective Storage of Electrons in Water by the Formation of Highly Reduced Polyoxometalate Clusters. *J. Am. Chem. Soc.* **2022**, *144* (20), 8951−8960.
(28) Petrus, E.; Garay-Ruiz, D.; Reiher, M.; Bo, C. Multi-Time-Scale Simulation of Complex Reactive Mixtures: How Do Polyoxometalates Form? *J. Am. Chem. Soc.* **2023**, *145* (34), 18920−18930.
(29) Petrus, E.; Segado, M.; Bo, C. Nucleation Mechanisms and Speciation of Metal Oxide Clusters. *Chem. Sci.* **2020**, *11* (32), 8448−8456.
(30) Vilà-Nadal, L.; Rodríguez-Fortea, A.; Yan, L. K.; Wilson, E. F.; Cronin, L.; Poblet, J. M. Nucleation Mechanisms of Molecular Oxides: A Study of the Assembly-Dissassembly of $[W_6O_{19}]^{2-}$ by Theory and Mass Spectrometry. *Angew. Chem., Int. Ed.* **2009**, *48* (30), 5452−5456.
(31) Petrus, E.; Buils, J.; Garay-Ruiz, D.; Segado-Centellas, M.; Bo, C. POMSimulator: An Open-Source Tool for Predicting the Aqueous Speciation and Self-Assembly Mechanisms of Polyoxometalates. *J. Comput. Chem.* **2024**, *45*, 2242.
(32) López, X.; Carbó, J. J.; Bo, C.; Poblet, J. M. Structure, Properties and Reactivity of Polyoxometalates: A Theoretical Perspective. *Chem. Soc. Rev.* **2012**, *41* (22), 7537.
(33) Bo, C.; Miró, P. On the Electronic Structure of Giant Polyoxometalates: Mo132vs. W72Mo60. *Dalton Trans.* **2012**, *41* (33), 9984.
(34) Kuepper, K.; Derks, C.; Taubitz, C.; Prinz, M.; Joly, L.; Kappler, J.-P.; Postnikov, A.; Yang, W.; Kuznetsova, T. V.; Wiedwald, U.; Ziemann, P.; Neumann, M. Electronic Structure and Soft-X-Ray-Induced Photoreduction Studies of Iron-Based Magnetic Polyoxometalates of Type {(M)M5}12FeIII30 (M = MoVI, WVI). *Dalton Trans.* **2013**, *42* (22), 7924.

https://doi.org/10.1021/acs.inorgchem.4c04497
Inorg. Chem. 2025, 64, 2716−2722

(35) Melgar, D.; Bandeira, N. A. G.; Bo, C. Electronic Structure Studies on the Whole Keplerate Family: Predicting New Members. *Chem.—Eur. J.* **2017**, *23* (22), 5338−5344.
(36) Mitra, T.; Miró, P.; Tomsa, A.; Merca, A.; Bögge, H.; Ávalos, J.; Poblet, J. M.; Bo, C.; Müller, A. Gated and Differently Functionalized (New) Porous Capsules Direct Encapsulates' Structures: Higher and Lower Density Water. *Chem.—Eur. J.* **2009**, *15* (8), 1844−1852.
(37) Garcia-Ratés, M.; Miró, P.; Müller, A.; Bo, C.; Avalos, J. B. Encapsulated Water Inside Mo $_{132}$ Capsules: The Role of Long-Range Correlations of about 1 Nm. *J. Phys. Chem. C* **2014**, *118* (10), 5545−5555.
(38) Watfa, N.; Melgar, D.; Haouas, M.; Taulelle, F.; Hijazi, A.; Naoufal, D.; Avalos, J. B.; Floquet, S.; Bo, C.; Cadot, E. Hydrophobic Effect as a Driving Force for Host−Guest Chemistry of a Multi-Receptor Keplerate-Type Capsule. *J. Am. Chem. Soc.* **2015**, *137* (17), 5845−5851.
(39) Bader, R. *Atoms in Molecules — a Quantum Theory International Series of Monographs on Chemistry*; Clarendon Press, 1994; Vol. *360*.
(40) Rodríguez, J. I.; Bader, R. F. W.; Ayers, P. W.; Michel, C.; Götz, A. W.; Bo, C. A High Performance Grid-Based Algorithm for Computing QTAIM Properties. *Chem. Phys. Lett.* **2009**, *472* (1−3), 149−152.
(41) te Velde, G.; Bickelhaupt, F. M.; Baerends, E. J.; Fonseca Guerra, C.; van Gisbergen, S. J. A.; Snijders, J. G.; Ziegler, T. Chemistry with ADF. *J. Comput. Chem.* **2001**, *22* (9), 931−967.
(42) Becke, A. D. Density-Functional Exchange-Energy Approximation with Correct Asymptotic Behavior. *Phys. Rev. A* **1988**, *38* (6), 3098−3100.
(43) Perdew, J. P. Density-Functional Approximation for the Correlation Energy of the Inhomogeneous Electron Gas. *Phys. Rev. B:Condens. Matter Mater. Phys.* **1986**, *33* (12), 8822−8824.
(44) Perdew, J. P. Erratum: Density-functional approximation for the correlation energy of the inhomogeneous electron gas. *Phys. Rev. B:Condens. Matter Mater. Phys.* **1986**, *34* (10), 7406.
(45) Lenthe, E. v.; Baerends, E. J.; Snijders, J. G. Relativistic Regular Two-component Hamiltonians. *J. Chem. Phys.* **1993**, *99* (6), 4597−4610.
(46) Van Lenthe, E.; Baerends, E. J. Optimized Slater-type Basis Sets for the Elements 1−118. *J. Comput. Chem.* **2003**, *24* (9), 1142−1156.
(47) Klamt, A. Conductor-like Screening Model for Real Solvents: A New Approach to the Quantitative Calculation of Solvation Phenomena. *J. Phys. Chem.* **1995**, *99* (7), 2224−2235.
(48) Álvarez-Moreno, M.; de Graaf, C.; López, N.; Maseras, F.; Poblet, J. M.; Bo, C. Managing the Computational Chemistry Big Data Problem: The ioChem-BD Platform. *J. Chem. Inf. Model.* **2015**, *55* (1), 95−103.

https://doi.org/10.1021/acs.inorgchem.4c04497
Inorg. Chem. 2025, 64, 2716−2722